NASA Technical Memorandum 107323

Single-Shot Spectrally Resolved UV Rayleigh Scattering Measurements in High Speed Flow

Richard G. Seasholtz
Lewis Research Center
Cleveland, Ohio

Prepared for the
Eighth International Symposium on Applications
of Laser Techniques to Fluid Mechanics
sponsored by the Instituto Superior Técnico
Lisbon, Portugal, July 8–11, 1996

National Aeronautics and
Space Administration

SINGLE-SHOT SPECTRALLY RESOLVED UV RAYLEIGH SCATTERING MEASUREMENTS IN HIGH SPEED FLOW

Richard G. Seasholtz

NASA Lewis Research Center
Cleveland, OH 44135, U.S.A.

ABSTRACT

A single-shot UV molecular Rayleigh scattering technique to measure velocity in high speed flow is described. The beam from an injection-seeded, frequency quadrupled Nd:YAG laser (266 nm) is focused to a line in a free air jet with velocities up to Mach 1.3. Rayleigh scattered light is imaged through a planar mirror Fabry-Perot interferometer onto a CCD array detector. Some laser light is also simultaneously imaged through the Fabry-Perot to provide a frequency reference. Two velocity measurements are obtained from each image. Multiple-pulse data are also given. The Rayleigh scattering velocity data show good agreement with velocities calculated from isentropic flow relations.

1. INTRODUCTION

Rayleigh scattering offers a means to measure gas flow parameters including density, temperature, and velocity. Since Rayleigh scattering is a molecular scattering process, no seeding of the flow is necessary. The Rayleigh scattered power is proportional to the gas density, the spectral width is related to the gas temperature, and the shift in the frequency of the spectral peak is proportional to one component of the bulk velocity. We have used this technique in a variety of aerospace applications including rocket exhaust plumes [Seasholtz *et al* (1991)] and wind tunnels [Kourous and Seasholtz (1993), Seasholtz *et al* (1995)]. This previous work used visible laser light, either the 488 or 514 nm lines of an argon-ion laser, or the 532 nm second harmonic of a Nd:YAG laser. There is considerable interest in using shorter wavelengths for two reasons. First, the Rayleigh scattering cross section varies as the inverse fourth power of wavelength. Thus the number of Rayleigh scattered photons will be higher by a factor of eight for a given laser power if the wavelength is halved. (Where the effect of the photon energy has been taken into account.) The second reason for using short wavelengths is that the reflectivity of metallic surfaces is generally less that it is at longer wavelengths. This is of particular interest in confined flow situations, such as small wind tunnels and aircraft engine components, where the stray laser light scattered from windows and internal surfaces in the test facility is a limiting factor in the application of Rayleigh scattering diagnostics. The previous study by Seasholtz *et al* (1995) used an iodine absorption cell [the filtered Rayleigh scattering technique developed by Miles *et al* (1991)] to block stray laser light. This approach, however, is more complex in that it requires that the laser frequency be tuned to a specific frequency in an iodine absorption line.

In this paper, we present the results of an initial study to use molecular Rayleigh scattering of the 266 nm fourth harmonic of a pulsed Nd:YAG laser for measuring velocity in a high speed air flow. The frequency of the Rayleigh scattered light is analyzed with a planar mirror Fabry-Perot interferometer used in a static imaging mode, with the images recorded on a cooled, high quantum efficiency CCD. The image consists of concentric interference fringes, where the fringe radii are Doppler-shifted by the bulk velocity of the fluid and are broadened by the thermal motion of the molecules. In addition, some unshifted light from the same laser pulse is also imaged through the interferometer to generate a reference fringe pattern, which is used to obtain the interferometer phase and finesse for the incident light. Any pulse-to-pulse variation in the laser frequency is accounted for since the Rayleigh and reference images are obtained from the same laser pulse. Small subregions located on the interference fringes of the Rayleigh scattered light are then analyzed using a least squares fit to the model function. Data are shown for measurements obtained with single laser pulses in a free jet with velocities up to Mach 1.3. Multiple laser pulse data are also given. In addition, data are presented for measured reflectivity of stainless steel and aluminum at 266 nm and 532 nm.

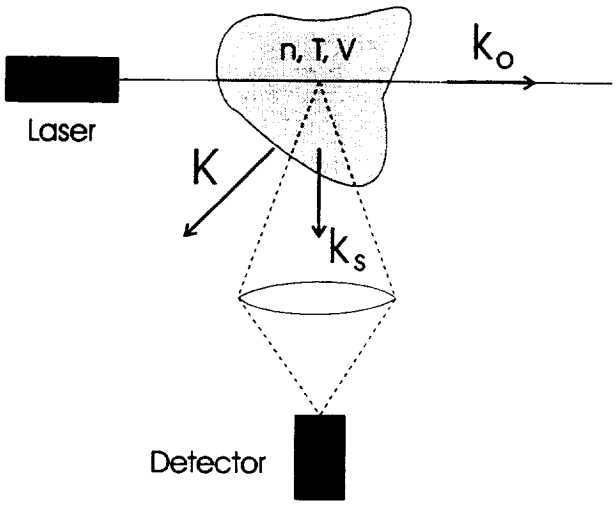

Fig. 1 - Light scattering experiment; $\mathbf{k}_o$ and $\mathbf{k}_s$ are wavevectors of incident beam and scattered beams; scattering wave vector $\mathbf{K} = \mathbf{k}_s - \mathbf{k}_o$.

2. THEORY

2.1 Rayleigh scattering

Rayleigh scattering [Young (1982)] is a result of the interaction of an electric field with an atom or molecule. Because the wavelength is much larger than the size of a molecule, a dipole moment is induced that oscillates and radiates at the frequency of the incident field. This is an elastic scattering process, where the internal energy of the molecule is not changed, so the frequency of the scattered light is equal to the frequency of the incident light altered only by the Doppler effect due to the motion of the molecules. Because of the random spatial distribution of the molecules in a gas, the total intensity of the scattered light from a volume of gas is the sum of the intensities of the light scattered from the individual molecules. At low gas densities, molecular interactions are rare and the Rayleigh scattering spectrum is determined only by the molecular velocity distribution; for the usual Maxwellian velocity distribution, the spectrum is thus a simple Gaussian. However, at higher gas density, the molecular motions become correlated and the character of the spectrum changes. The spectrum can be analyzed either by considering the scattering from the individual molecules with proper accounting of the collective effects or by considering the scattering as being caused by fluctuations in the gas density.

The number of detected photoelectrons collected by an optical system with solid collection angle Ω (fig. 1)

$$N_R = \frac{\varepsilon E_o n L_x \lambda \Omega}{hc}\left(\frac{d\sigma}{d\Omega}\right)\sin^2\chi \qquad (1)$$

where λ is the laser wavelength, E_o is the laser energy, n is the gas number density, L_x is the length along the beam of the scattering volume, $d\sigma/d\Omega$ the differential scattering cross section, χ is the angle between the electric field vector of the (linearly polarized) incident light and the direction of the scattered light, ε is the overall collection efficiency (including the detector quantum efficiency), h is Planck's constant, and c is the velocity of light. The Rayleigh differential scattering cross section is related to the index of refraction μ of the gas by

$$\left(\frac{d\sigma}{d\Omega}\right) = \frac{4\pi^2}{\lambda^4 n^2}(\mu - 1)^2 \qquad (2)$$

Since the refractive index of most gases is only weakly dependent on the wavelength, we see that the scattering cross section varies as the inverse fourth power of the wavelength. This strong dependence on wavelength is illustrated by the blue color of the sky, where shorter wavelength blue light is more strongly scattered than the longer wavelengths in the solar spectrum. For flow diagnostics, use of short wavelength ultraviolet lasers has obvious benefits. In addition to the much stronger scattering intensities, operating in the UV should reduce the problem of stray laser light because the reflectivity of metals tends to be less than at shorter wavelengths. This advantage, however, is offset by the reduction of available laser power in the UV. For example, in our Nd:YAG laser the pulse energy is reduced from about 800 mJ at 532 nm to about 80 mJ at 266 nm. In addition, the quantum efficiency of detectors is also less in the UV. Our back-illuminated CCD has a quantum efficiency of 70 % at 532 nm, but is only about 25 % at 266 nm. Another consideration is the availability of high quality imaging optics for UV operation. For the work reported here, we used the ubiquitous 105 mm focal length, f/4.5 35-mm camera lens. Taking all these factors in consideration leads to the conclusion that, considering only the Rayleigh scattering signal, one is better off using the longer wavelength. This would be the case for open flows, such as free jets and larger wind tunnels, where one can easily control stray laser light. On the other hand, in confined flow experiments, control of stray laser light is much more difficult because of the close proximity of the measurement region to windows and metallic surfaces. In this case, the lower Rayleigh scattering signal level is more than offset by the increase in the ratio of Rayleigh scattering signal to stray laser light.

The shape of the Rayleigh scattering spectrum is determined by the gas density and scattering angle. We define, as is customary, a non-dimensional collision frequency $y = p/\eta Ka$ where p is the gas pressure, η is the shear viscosity, $K = (4\pi/\lambda)\sin(\theta_s/2)$ is the magnitude of the interaction wave vector $\mathbf{K} = \mathbf{k}_s - \mathbf{k}_o$ (with $\mathbf{k}_o$ and $\mathbf{k}_s$ being the wave vectors of the incident and scattered light), θ_s is the scattering angle, and $a = (2\kappa T/m)^{1/2}$ is the most probable molecular speed (with κ being Boltzmann's constant, m the molecular mass, and T the gas temperature). Thus y is the optical frequency shift and collision frequency ($\sim p/\eta$) normalized with respect to Ka, which is on the order of the frequency of a sound wave in the gas with wavelength $\Lambda_s = 2\pi/K$. (Note that $a = c_s(2/\gamma)^{1/2}$, where c_s is the speed of

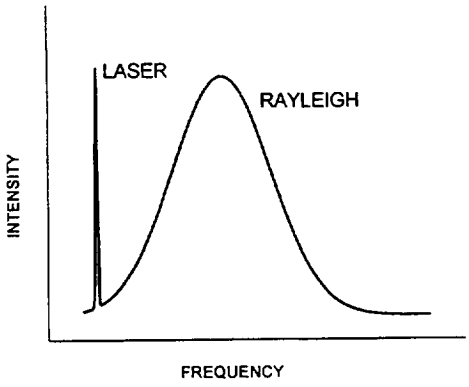

Fig. 2 - Rayleigh scattering spectrum showing thermal broadening and shift caused by bulk velocity.

sound and γ is the ratio of specific heats.) Alternatively, y can be interpreted as the ratio of the acoustic wavelength Λ_s to the molecular mean free path.

For a single-component, low density gas, where $y<<1$, the normalized spectrum of the Rayleigh scattered light is given by the Gaussian (fig. 2)

$$S(f-f_o)\,df = \frac{1}{\sqrt{\pi}\,aK}\exp\left\{-\left[\frac{2\pi\,(f-f_o)-\mathbf{K}\cdot\mathbf{u}}{aK}\right]^2\right\}df \quad (3)$$

where f_o is the laser frequency and $\mathbf{u}$ is the mean gas velocity. As shown in figure 2, the spectral peak is shifted by a frequency proportional to the component of the bulk velocity in the $\mathbf{K}$ direction. The spectral width is proportional to the square root of the gas temperature.

Note that in this limiting case for low density gases, the spectral shape is not a function of the y parameter. However, for higher density gases (where $y \sim 1$), the spectrum is no longer Gaussian and is a function of the y parameter. For $y >> 1$ (high density gases), the scattering spectrum is strongly influenced by collective effects and is characterized by a central peak and two sidebands. The sidebands can be thought of as being caused by scattering from thermally excited random acoustic waves and is referred to as the Brillouin-Mandelstam doublet [Young (1982)]. A continuum theory, such as given by Clark (1975) can be used to model the spectrum here. The spectral shape in this regime is only a function of the y parameter. However, the spectrum in the transition regime, where $y \sim 1$, requires a more detailed kinetic theory. We used the *S6* model developed by Tenti *et al* (1974) for our work. This model requires the shear viscosity, the thermal conductivity, the internal specific heat, and the bulk viscosity of the gas. In all cases, the Rayleigh scattering spectral shape is a function of the gas thermodynamic properties, which forms the basis for a diagnostic to measure gas density, temperature, and velocity.

The Rayleigh scattered light collected from one vantage point contains sufficient information to determine the gas density, temperature, and one component of the bulk velocity. (Spectra measured at other $\mathbf{K}$ vectors would give other velocity components.) Density is proportional to the total Rayleigh scattering as given by equation 1. This, however, generally requires calibration to determine the proportionality constant. (Although it is also possible to determine the density from the spectral shape for a limited range of y parameters values, as shown by Lock *et al* (1992)).

2.2 Measurement of Rayleigh Scattering Spectrum

Because the Rayleigh linewidth is on the order of one GHz, a very high spectral resolution instrument is required. Conventional grating spectrometers generally do not have adequate resolution. A Fabry-Perot interferometer, either confocal or planar mirror type, can provide the needed resolution and is the most common instrument used for Rayleigh scattering studies. Both scanning techniques and imaging techniques have been used. In the scanning mode the passband of the interferometer is scanned across the Rayleigh spectrum by varying either the mirror spacing or the pressure of the gas in the Fabry-Perot cavity. This method is limited to time average measurements, usually at a single point in the flow. With the imaging technique, a region of the fluid illuminated by a laser beam is imaged through the interferometer onto an array detector, usually a CCD camera. As discussed below, the intensity of the recorded image is a function of the Rayleigh spectrum and the interferometer transmission function. Two features of this technique compared to scanning measurements are (1) a single image can give measurements at a number of locations in the flow and (2) these measurements can be made with a single laser pulse, giving instantaneous measurements. One problem with the Fabry-Perot used in a single pass mode is its limited selectivity, which means that it is unable to measure a weak signal in the presence of a strong interfering signal. This, unfortunately, is the situation encountered when using Rayleigh scattering diagnostics in small enclosed flows, where a large amount of stray light exists due to scattering from windows and solid surfaces.

2.3 Fabry-Perot interferometer

The Fabry-Perot interferometer (fig. 3) consists of two partially transmitting planar mirrors, which act as a multiple beam interference device. Multiple reflections between the mirrors result in a transmission function (defined as the fraction of light transmitted by Fabry-Perot for a monochromatic source) [Vaughan (1989)].

$$I_{FP}(\psi) = \left[1 + F\sin^2\left(\frac{\psi}{2}\right)\right]^{-1} \quad (4)$$

where ψ is the phase change (neglecting any phase change on reflection) of the light between successive reflections given by

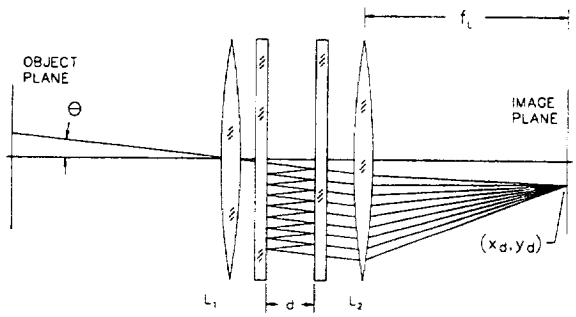

Fig. 3 - Fabry-Perot interferometer; single ray from point on object plane is imaged to single point on image plane; L_1 is collimating lens and L_2 is fringe forming lens.

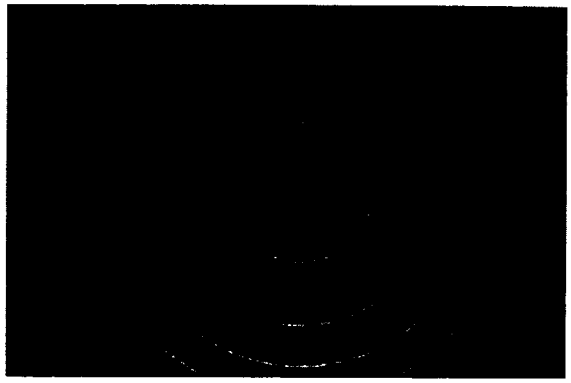

Fig. 4 - Fabry-Perot interference pattern of single frequency light from extended source.

$$(f,\theta_r) = \frac{4\pi f \mu d \cos\theta_r}{c} \qquad (5)$$

Here, $f=c/\lambda_o$ is the optical frequency, μ is the refractive index of the medium in the Fabry-Perot cavity, d is the Fabry-Perot mirror spacing, θ_r is the angle between the ray and the optic axis, and $F = 1/(\sin^2(\pi/2N_E)$ where N_E is the effective finesse. The image of a monochromatic extended source located in the object plane consists of a series of unequally spaced concentric rings, such as shown in figure 4. With the innermost fringe located on the optical axis (i.e., having zero radius), the other fringe radii are given $r_n = f_L(n\lambda_o/d)^{1/2}$ for $n = 1,2,3,\cdots$, where f_L is the focal length of the fringe forming lens. Note that although the fringes are unequally spaced, their frequency separations are all equal to the free spectral range $FSR=c/2d$.

The Fabry-Perot interferometer can be used in the static, imaging mode, which takes advantage of the angular sensitivity of the transmission to achieve frequency resolution (see eq. 5). In this method a region of the flow illuminated with laser light is imaged through the Fabry-Perot onto an array detector. The fringe location is radially shifted and broadened by an amount related to the frequency shift and spectral shape of the scattered light (the fringes move outward as the frequency increases). The spectrum can only be measured over a spatial region that includes part of an interference fringe. (Note that there is a one-to-one correspondence between an object point in the flow and an image point in the fringe plane.) This results in a measurement that is spatially averaged over that region. However, with several fringes in the field of view, measurements can be obtained at a large number of locations. This imaging method is the basis for the technique described in this paper.

2.4 Model of Rayleigh spectral measurements using Fabry-Perot interferometer

Small subregions located on the interference fringes of the Rayleigh scattered light are then analyzed using a least squares fit to the model function

$$\langle N_{Dq}\rangle = \int_{\Omega}\int_{\Delta f}\int_{-\infty}^{\infty} [A_R S_R(f,\Omega) + A_W \delta(f-f_o)] I_{FP}(f,\theta_r)\, df\, dA\, d\Omega + B_q \qquad (6)$$

where $\langle N_{Dq}\rangle$ is the expected number of detected photons for the q^{th} pixel, A_R is the total amount of Rayleigh scattering that would be detected by the q^{th} pixel if the Fabry-Perot interferometer were not present, and θ_r is the angle of the light ray with the optical axis. A_W represents the unshifted laser light scattered from windows and walls at the laser frequency $f_o=c/\lambda_o$. The spectrum of the Rayleigh scattered light is $S_R(f,\Omega)$ and $I_{FP}(f,\theta_r)$ is the Fabry-Perot instrument function. Broadband background light, detector dark current, and readout noise are represented by B_q. The integration over the solid angle is necessary to account for the range of **K** vectors over the light collection aperture. The *S6* model developed by Tenti *et al* (1974) is used for the spectrum.

3. EXPERIMENT

3.1 Optical setup

The optical setup is shown in figures 5 and 6. The beam from an injection-seeded, frequency-quadrupled, Nd:YAG laser with 70 mJ pulse energy and 10 Hz pulse rate was focused with a 200 mm focal length lens. To avoid air breakdown, the lens was intentionally misaligned to introduce some aberrations. The beam crossed the nozzle axis at 45°, and the beam size at the measurement location was approximately 150 μm. This Rayleigh scattered light was collected at a 90° scattering angle and collimated with a 250 mm focal length lens. The light was then passed through a 3.2 mm thick uncoated fused silica beamsplitter and the Fabry-Perot interferometer. A commercially available Fabry-Perot interferometer was used. The mirrors (70 mm diameter, λ/200 flatness, and 90% reflectivity at 266 nm) were set at a 7.50 mm spacing for the measurements reported

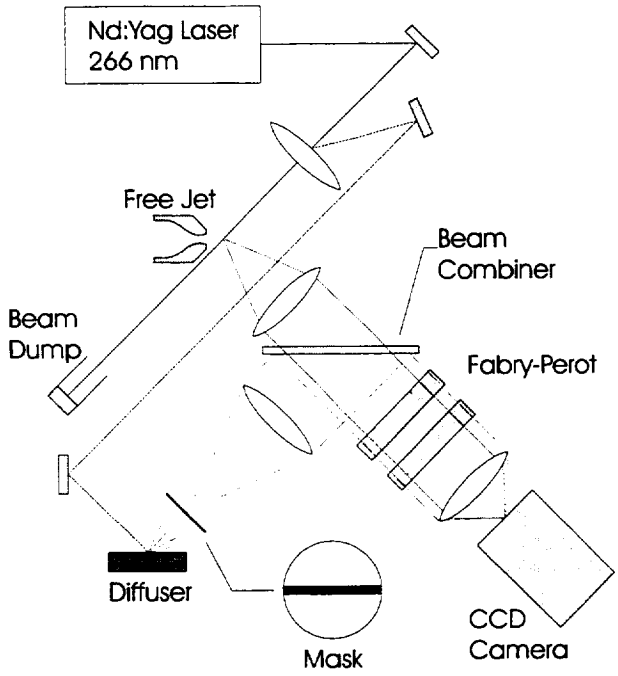

Fig. 5 - Optical layout of Rayleigh scattering experiment; see figure 6 for details.

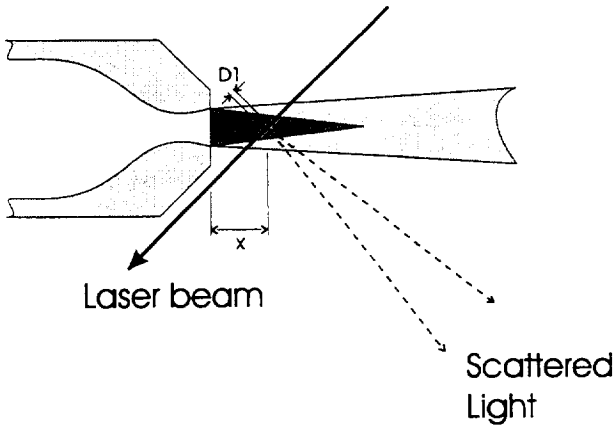

Fig. 6 - Detail view of Rayleigh scattering measurement region; x is the distance from the nozzle exit plane to the measurement region; D_1 is the separation between the two measurement obtained from each image.

here, which corresponded to free spectral range (FSR) of about 20 GHz. The light emerging from the Fabry-Perot was focused onto the detector (liquid nitrogen cooled, back illuminated, CCD array with 1752 x 532 15 μm square pixels, 25% quantum efficiency at 266 nm) by a 105 mm focal length, f/4.5, 35 mm UV camera lens. Note that use of this relatively slow lens with an aperture of only 23 mm means that the full 70 mm aperture of the Fabry-Perot is not used. To reduce data storage requirements, only a 200 x 200 pixel region of the CCD was used, which gave a field of

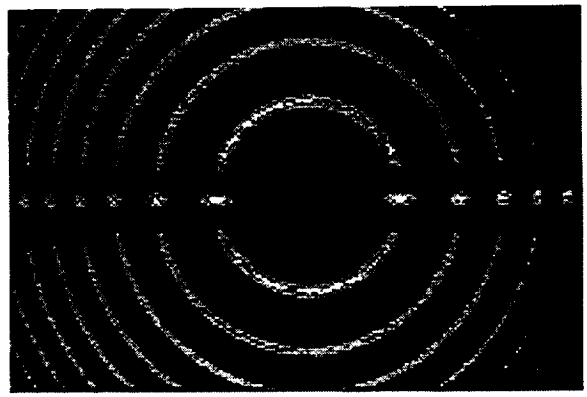

Fig. 7 - Fabry-Perot interferometer image showing reference light (upper and lower) and Rayleigh scattering light (center).

view in the flow of 7.1 x 7.1 mm.. The images were digitized with a 14 bit A/D converter and transferred to a laboratory computer for storage and analysis.

To include the effects of laser shot-to-shot frequency variation and drift of the Fabry-Perot interferometer, reference data was simultaneously recorded along with the Rayleigh scattering data. Any pulse-to-pulse variation in the laser frequency thus is accounted for since the Rayleigh and reference images are obtained from the same laser pulse. This was accomplished by directing some of the unshifted laser light onto a diffusely scattering aluminum surface. A 100 mm focal length lens collimated the light from the diffuser, which was directed into the Fabry-Perot via the beamsplitter. A 0.30 mm diameter wire was placed in the focal plane of the 100 mm lens. This served to block unshifted Nd:YAG light in the reference path from a horizontal strip in the CCD image; the blocked area comprised about 12 % of the total number of rows of pixels. For single-shot data, the camera was operated with a shutter speed of 0.1 sec. A 1 sec exposure was used for the multiple-shot data (giving a 10 pulse average). The test cell lights were turned off to limit ambient background light. Figure 7 shows a typical image with the Rayleigh scattered light along the center line and the Nd:YAG reference light in the upper and lower parts of the image. The reference fringes are only broadened by the instrument response function of the interferometer, while the Rayleigh scattering fringes are also Doppler-shifted by the bulk velocity of the fluid and are broadened by the thermal motion of the molecules.

3.2 Test nozzle

The Mach 1.3 supersonic nozzle had an exit diameter of 9.3 mm. The air supply was filtered with a 0.2 μm filter to remove particles. Data were obtained at subsonic velocities and at Mach 1.3. The plenum pressure was measured with an electronic pressure meter and the isentropic flow equations were used to calculate the exit velocity.

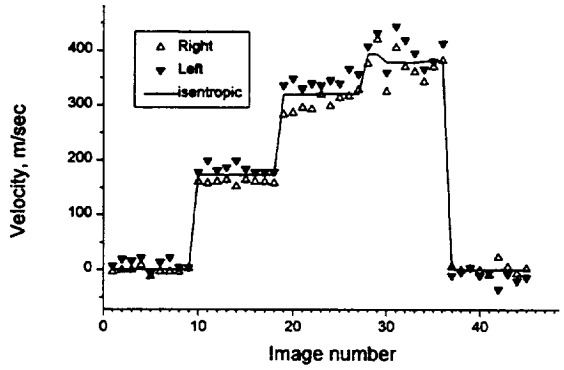

Fig. 8 - Single-shot velocity measurements in free jet; nine images taken at each of 3 flow conditions (with zero velocity condition at beginning and end); distance from nozzle exit x = 15 mm; two measurements/image with separation D_I = 1.8 mm; velocity calculated for isentropic flow also shown. (note that flow was not constant during each condition).

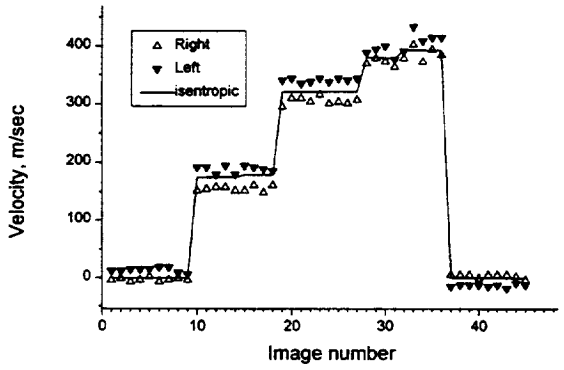

Fig. 9 - Ten-shot average velocity measurements in free jet x=15 mm from exit plane; two measurements/image with separation D_I= 1.8 mm; velocity calculated for isentropic flow also shown.

3.3 Data processing

The data reduction procedure was as follows. The first step was to analyze the upper and lower regions to determine both the Fabry-Perot interferometer phase and finesse. (The measured finesse includes the effect of the finite linewidth of the Nd:YAG laser.) This was done by using a least-squares fit of the image to a model function for the Nd:YAG reference fringes (eq. 6 with A_R = 0). This fit gives the coordinates of the center of the fringe pattern. Four 15 x 15 pixel subregions (equal to about a 0.54 mm square region in the flow) on the inner fringe (just outside the central band) are then analyzed to obtain reference values for the phase on the left and right sides of the central fringe (given by the mean of the upper and lower phases of the reference light). The Rayleigh scattering image is likewise analyzed to determine its phase at two locations on the inner fringe. The shift in the peak of the Rayleigh scattering fringe is related to the axial velocity component. The model function (eq. 6) was evaluated at 9 points in each pixel for the numerical integration over the area of each pixel. The flow direction was assumed to be along the tunnel axis for the purpose of converting the measured velocity component (which is along **K**) to the velocity magnitude. The *y* parameter was about 0.5, so the Tenti *S6* model for the Rayleigh spectrum was used.

Table 1 - Comparison of velocity measured by Rayleigh scattering and velocity calculated from isentropic flow relation; mean velocity and standard deviation in m/sec.

Single-shot data (see fig. 8)

Right	Left	Right+Left	Isentropic
159(4)	184(14)	172(14)	173
304(16)	344(11)	323(25)	320
373(29)	403(29)	388(32)	383

Ten-shot data (see fig. 9)

Right	Left	Right+Left	Isentropic
155(4)	188(6)	172(17)	176
306(6)	341(3)	323(19)	321
380(12)	403(17)	392(19)	387

4. RESULTS

4.1 Rayleigh scattering velocity measurements

Examples of Rayleigh scattering velocity measurements are shown in figures 8 and 9. The axial velocity component was measured near the jet center line for two subsonic velocities and for Mach 1.3 supersonic flow. Nine images were obtained at each flow condition, with a set of images at zero flow being taken at the beginning and the end of the experiment. Two velocities (separated by the inner fringe diameter $D_I \cong 2$ mm, as shown in fig. 6) were obtained from each image. Figure 8 shows data obtained with a single laser pulse. Figure 9 shows similar data obtained with 10 laser pulses. Also shown are velocities calculated from the ambient and plenum pressures and the total temperature using the isentropic flow relations [Ames Research Staff (1953)]. Note that the velocity was not necessarily constant at each flow condition because of variation in the air supply pressure. The statistical properties of the measured velocities are shown in Table 1. The two

Table 2 - Measured Reflectance of stainless steel and aluminum

316 Stainless Steel

incidence angle	266 nm	532 nm
4°	32%	58%
45°	44%	66%

Aluminum

incidence angle	266 nm	532 nm
4°	89%	93%
45°	94%	87%

velocities (labeled Right and Left) appear to have a systematic error that results in the two measurements being displaced in opposite directions from the isentropic velocity. The source of this error is not known at the present time. However, as shown in Table 1, the mean of the two measurements shows very good agreement with the isentropic velocity. It should be noted that no calibration was used. (The only measured parameters were the Fabry-Perot mirror spacing and the scattering angle.)

The standard deviation in the single-shot data (Right or Left) was about 15 m/sec for the two lower velocities and about 30 m/sec for the Mach 1.3 flow. One cause of the larger standard deviation in the Mach 1.3 flow is velocity variations caused by fluctuations in the air supply pressure. The high acoustic noise level, which can affect the stability of the Fabry-Perot (no acoustic shielding was used), could also contribute to the larger standard deviation. This larger variance is also evident in the ten-shot data.

4.2 Reflectance measurements of stainless steel and aluminum

The factor limiting Rayleigh scattering diagnostics in enclosed flows is frequently the amount of stray laser light resulting from scattering from surfaces in the test rig. We measured the reflectance of two materials commonly found in test facilities (316 stainless steel and aluminum) at 266 nm and 532 nm to determine if this scattering would less in the UV. The stainless steel was polished using a 1 μm diamond polishing compound, but showed some residual surface pits. The aluminum sample was evaporated onto a glass plate. The estimated thickness of the aluminum was 150 nm. The measurements were made by measuring the incident and reflected power with a thermal type power meter. Two angles of incidence were measured (45° and near normal). The results of these measurements are shown in Table 2. Note that the stainless steel reflectance is substantially lower at 266 nm compared to 532 nm. However, the aluminum did not show this reduction.

5. CONCLUDING REMARKS

The feasibility of using a UV laser for Rayleigh scattering velocity measurements was demonstrated. Signal levels were high enough to allow measurements with a single laser pulse. The use of the Fabry-Perot interferometer used in the static, imaging mode allows measurements to be made simultaneously at multiple locations in the flow. Although only two measurements per image were obtained here, it is possible to obtain many more. This capability could be used to measure spatial velocity correlations. Although the system described here measured a single velocity component, it could be extended in a straightforward manner to simultaneously measure two or three components. This could be done by adding one or two additional sets of collection optics at other scattering angles.

One difficulty in working in the UV is the small selection of imaging-quality optics. In this work, the collection optics solid angle was only f/11. The Fabry-Perot interferometer used here has 70 mm diameter mirrors. Use of the full Fabry-Perot aperture would increase the collection angle to f/3.6, which would increase the collected Rayleigh scattered light by an order of magnitude. Another consideration is the focal length of the fringe forming lens. A longer focal length results in a higher spatial resolution, which means the Rayleigh scattering spectrum can be more accurately measured.

One precaution that should be used with this technique in high acoustic noise environments is to provide sufficient acoustic shielding of the Fabry-Perot interferometer and the laser. Another highly desirable addition would be automatic control of the Fabry-Perot alignment. The present procedure involves manual adjustment of the Fabry-Perot to maintain alignment, which takes time during the test and requires a skilled operator.

6. ACKNOWLEDGMENTS

We would like to acknowledge the diligent efforts of Mr. W. Trevor John who was responsible for setting up and aligning the optical system.. Also, we thank Prof. G. Tenti for providing us with the computer code for his 6 moment Rayleigh scattering model.

7. REFERENCES

Ames Research Staff, 1953, Equations, Tables, and Charts for Compressible Flow, NACA Report 1135.

Clark, N.A. 1975, Inelastic Light Scattering from Density Fluctuations in Dilute Gases. The kinetic hydrodynamic transition in monatomic gas, *Phys. Rev.* A12, pp. 232-244.

Kourous, H.E. & Seasholtz, R.G. 1994, Fabry-Perot Interferometer Measurement of Static Temperature and Velocity for ASTOVL Model Tests, FED-Vol.1, Laser Anemometry - 1994: Advances and Applications, ASME.

Lock, J.A., Seasholtz, R.G., & John, W.T. 1992, Rayleigh-Brillouin Scattering to Determine One-Dimensional Temperature and Number Density Profiles of a Gas Flow Jet, Appl. Opt., vol. 31, no. 15, pp. 2839-2848.

Miles, R.B., Lempert, W.R. & Forkey, J. 1991, Instantaneous Velocity Fields and Background Suppression by Filtered Rayleigh Scattering, AIAA 29th Aerospace Sciences Meeting, Reno, AIAA paper 91-0357.

Seasholtz, R.G., Buggele, A.E., & Reeder, M.F. 1995, Instantaneous Flow Measurements in a Supersonic Wind Tunnel Using Spectrally Resolved Rayleigh Scattering, SPIE International Symposium on Optical Science, Engineering, and Instrumentation, San Diego, July 9-14.

Seasholtz, R.G., Zupanc, F.J., & Schneider, S.J. 1992, Spectrally Resolved Rayleigh Scattering Diagnostic for Hydrogen-Oxygen Rocket Plume Studies, J. Propulsion and Power, vol. 8, no.5, pp. 935-942.

Tenti, G., Boley, C.D., & Desai, R.C. 1974, On the Kinetic Model Description of Rayleigh Brillouin Scattering from Molecular Gases, Can. J. Phys. Vol. 52, pp. 285-290.

Vaughan, J.M. 1989, The Fabry Perot Interferometer, History, Theory, Practice and Applications, pp. 89-112, Adam Hilger, Bristol.

Young, A.T. 1982, Rayleigh Scattering, Physics Today, January (1982) pp. 42-48.

REPORT DOCUMENTATION PAGE

Form Approved
OMB No. 0704-0188

1. AGENCY USE ONLY (*Leave blank*)	2. REPORT DATE	3. REPORT TYPE AND DATES COVERED
	October 1996	Technical Memorandum

4. TITLE AND SUBTITLE

Single-Shot Spectrally Resolved UV Rayleigh Scattering Measurements in High Speed Flow

5. FUNDING NUMBERS

WU-505-62-50

6. AUTHOR(S)

Richard G. Seasholtz

7. PERFORMING ORGANIZATION NAME(S) AND ADDRESS(ES)

National Aeronautics and Space Administration
Lewis Research Center
Cleveland, Ohio 44135-3191

8. PERFORMING ORGANIZATION REPORT NUMBER

E-10426

9. SPONSORING/MONITORING AGENCY NAME(S) AND ADDRESS(ES)

National Aeronautics and Space Administration
Washington, D.C. 20546-0001

10. SPONSORING/MONITORING AGENCY REPORT NUMBER

NASA TM-107323

11. SUPPLEMENTARY NOTES

Prepared for the Eighth International Symposium on Applications of Laser Techniques to Fluid Mechanics sponsored by the Instituto Superior Técnico, Lisbon, Portugal, July 8–11, 1996. Responsible person, Richard G. Seasholtz, organization code 2520, (216) 433–3754.

12a. DISTRIBUTION/AVAILABILITY STATEMENT

Unclassified - Unlimited
Subject Category 35

This publication is available from the NASA Center for AeroSpace Information, (301) 621–0390.

12b. DISTRIBUTION CODE

13. ABSTRACT (*Maximum 200 words*)

A single-shot UV molecular Rayleigh scattering technique to measure velocity in high speed flow is described. The beam from an injection-seeded, frequency quadrupled Nd:YAG laser (266 nm) is focused to a line in a free air jet with velocities up to Mach 1.3. Rayleigh scattered light is imaged through a planar mirror Fabry-Perot interferometer onto a CCD array detector. Some laser light is also simultaneously imaged through the Fabry-Perot to provide a frequency reference. Two velocity measurements are obtained from each image. Multiple-pulse data are also given. The Rayleigh scattering velocity data show good agreement with velocities calculated from isentropic flow relations.

14. SUBJECT TERMS

Rayleigh scattering; Fabry-Perot interferometers

15. NUMBER OF PAGES

10

16. PRICE CODE

A02

17. SECURITY CLASSIFICATION OF REPORT	18. SECURITY CLASSIFICATION OF THIS PAGE	19. SECURITY CLASSIFICATION OF ABSTRACT	20. LIMITATION OF ABSTRACT
Unclassified	Unclassified	Unclassified	